Magnetic Resonance Imaging 109 (2024) 256–263

Contents lists available at ScienceDirect

Magnetic Resonance Imaging

journal homepage: www.elsevier.com/locate/mri

Fully automated contrast selection of joint bright- and black-blood late gadolinium enhancement imaging for robust myocardial scar assessment

Victor de Villedon de Naide [a], Jean-David Maes [b], Manuel Villegas-Martinez [a], Indra Ribal [a], Aurélien Maillot [a], Valéry Ozenne [a], Géraldine Montier [b], Thibaut Boullé [b], Soumaya Sridi [b], Pauline Gut [a,c], Thomas Küstner [d], Matthias Stuber [a,c,e], Hubert Cochet [a,b], Aurélien Bustin [a,b,c,*]

[a] Université de Bordeaux, INSERM, CRCTB, U 1045, IHU Liryc, F-33000 Bordeaux, France
[b] CHU de Bordeaux, Department of Cardiovascular Imaging, INSERM, U 1045, F-33000 Bordeaux, France
[c] Department of Diagnostic and Interventional Radiology, Lausanne University Hospital and University of Lausanne, Lausanne, Switzerland
[d] Medical Image and Data Analysis (MIDAS.lab), Department of Diagnostic and Interventional Radiology, University Hospital of Tübingen, 72076 Tübingen, Germany
[e] Center for Biomedical Imaging (CIBM), Lausanne, Switzerland

ARTICLE INFO

Keywords:
Cardiac MRI
Black-blood imaging
Late gadolinium enhancement
Inversion time
Myocardial scar

ABSTRACT

Purpose: Joint bright- and black-blood MRI techniques provide improved scar localization and contrast. Black-blood contrast is obtained after the visual selection of an optimal inversion time (TI) which often results in uncertainties, inter- and intra-observer variability and increased workload. In this work, we propose an artificial intelligence-based algorithm to enable fully automated TI selection and simplify myocardial scar imaging.
Methods: The proposed algorithm first localizes the left ventricle using a U-Net architecture. The localized left cavity centroid is extracted and a squared region of interest ("focus box") is created around the resulting pixel. The focus box is then propagated on each image and the sum of the pixel intensity inside is computed. The smallest sum corresponds to the image with the lowest intensity signal within the blood pool and healthy myocardium, which will provide an ideal scar-to-blood contrast. The image's corresponding TI is considered optimal. The U-Net was trained to segment the epicardium in 177 patients with binary cross-entropy loss. The algorithm was validated retrospectively in 152 patients, and the agreement between the algorithm and two magnetic resonance (MR) operators' prediction of TI values was calculated using the Fleiss' kappa coefficient. Thirty focus box sizes, ranging from 2.3mm^2 to 20.3cm^2, were tested. Processing times were measured.
Results: The U-Net's Dice score was 93.0 ± 0.1%. The proposed algorithm extracted TI values in 2.7 ± 0.1 s per patient (vs. 16.0 ± 8.5 s for the operator). An agreement between the algorithm's prediction and the MR operators' prediction was found in 137/152 patients ($\kappa = 0.89$), for an optimal focus box of size 2.3cm^2.
Conclusion: The proposed fully-automated algorithm has potential of reducing uncertainties, variability, and workload inherent to manual approaches with promise for future clinical implementation for joint bright- and black-blood MRI.

1. Introduction

Bright-blood (BR) late gadolinium enhancement (LGE) imaging is the cornerstone technique for the assessment of regional scar formation and myocardial injury [1,2]. The presence, extent, and distribution of LGE are key features to assess the etiological diagnosis in acute coronary syndromes, chronic structural heart disease, or ventricular arrhythmias or to appreciate the prognosis in patients with structural heart disease [3]. The strength of the method lies in its ability to provide high contrast between healthy and injured myocardium, thanks to an inversion recovery mechanism that blackens the surrounding healthy tissue [4].

Despite the excellent above-mentioned property, bright pixels from the blood pool often induce a limited contrast between myocardial lesions and the blood pool present in the adjacent chambers, making subendocardial scars challenging to detect. This lack of contrast can be critical as the size, localization, and transmurality of the scar within the cardiac anatomy are key factors guiding the patients' treatments [5]. To circumvent this problem, black-blood (BL)-LGE imaging has been

* Corresponding author at: Université de Bordeaux, INSERM, CRCTB, U 1045, IHU Liryc, F-33000 Bordeaux, France.
E-mail address: aurelien.bustin@ihu-liryc.fr (A. Bustin).

https://doi.org/10.1016/j.mri.2024.03.035
Received 4 September 2023; Received in revised form 14 March 2024; Accepted 21 March 2024
Available online 23 March 2024

developed for improved scar detection, promoting the appearance of new studies in high-quality vessel wall visualization and myocardial scar imaging [6,7]. These technologies were followed by the development of joint BR- and BL-LGE techniques, which simultaneously provide improved scar contrast (from BL-LGE images) and detailed cardiac anatomy information (from BR-LGE images) [5,8].

In clinical practice, the manual selection of an inversion time (TI) parameter by magnetic resonance (MR) operators is required for both conventional BR-LGE imaging and BL-LGE imaging. This TI parameter represents the delay between the preparation pulse and the data acquisition, and its accurate selection is crucial for achieving optimal contrast between scar tissue and blood or healthy myocardium on the BL-LGE images. However, the manual and expert-dependent TI selection process is associated with several drawbacks, including TI uncertainties, inter- and intra-observer variability, increased workload for MR operators, and complexity of the examination [9]. These limitations have hindered the widespread adoption of joint BR- and BL-LGE imaging in clinical routine.

Recent advancements in artificial intelligence (AI) are promising in automating TI selection for conventional BR-LGE imaging [10,11]. However, no algorithm has fully automated this process in joint BR- and BL-LGE imaging. Therefore, achieving operator-free TI selection would represent a significant step towards enhancing the robustness, reproducibility, simplicity, and fully automation of myocardial scar imaging.

The primary objectives of this study were twofold: first, to enable MR operator-free joint BR- and BL-LGE imaging by leveraging AI to fully automate TI selection process; and second, to rigorously validate the performance of this method in patients with structural heart disease.

2. Material and methods

2.1. Image acquisition

Acquisitions were performed on a 1.5 T system (Siemens, MAGNETOM Aera, Erlangen, Germany) using an 18-element body coil and a 32-element spine coil. Short-axis 2D interleaved joint BR- and BL-LGE images were collected using the recently proposed Scar-specific imaging with Preserved myOcardial visualizaTion (SPOT) sequence [5]. SPOT is a single-shot LGE sequence combining inversion recovery and T1-rho preparation pulses to jointly collect BL-LGE (odd heartbeats) and BR-LGE (even heartbeats) images. Whole-heart images were acquired under breath-holds 15 min post intravenous injection of 0.1 mmol/kg gadoterate meglumine (Dotarem®, Guerbet). Four single-shot images were collected per slice position and were averaged to reach a higher signal-to-noise ratio [1,12,13]. Acquisition parameters are provided in Table 1. A dedicated free-breathing SPOT scout sequence was played out prior to the whole-heart acquisition to find the TI providing a nulling of both healthy myocardium and blood signals. This sequence collected 14 mid-ventricular BL-LGE images with increasing TIs (ranging from 60 ms to 190 ms with a 10 ms increment) in the odd heartbeats and 14 BR-LGE images in the even heartbeats in a scan time of 28 heartbeats (Fig. 1A). An example of BL-LGE TI-scout images collected in two patients with myocardial infarction is provided in Supporting information Fig. S1.

2.2. Fully automated TI selection

The algorithm emulates the conventional process of TI selection by automatically identifying, from a prior TI-scout sequence, the image with the darkest blood and healthy myocardium signals. To achieve this, the algorithm has to i) localize the left ventricle (LV) within the image series, and then ii) perform an analysis of pixel intensities to identify the image with the optimal contrast. The proposed algorithm was organised in three steps detailed hereafter (Fig. 1B).

Step 1: LV localization. A U-Net architecture (Fig. 2) [14] was implemented to segment the epicardium on the first BR-LGE image collected from the TI-scout sequence. The U-Net was designed with four multi-scale encoder/decoder parts, with concatenation layers connecting features from the encoder and the decoder.

Step 2: Focus box propagation. Once the centroid of the segmentation is extracted on the first BR-LGE image collected, a squared region of interest is created around the resulting pixel ("focus box"). Then, the focus box is propagated, with the same coordinates, on each BL-LGE image collected with different TIs.

Step 3: Signal analysis. The sum of pixel intensities within these focus boxes was computed for each TI image. The smallest sum corresponded to the TI image with the darkest blood signal, and the corresponding TI was then selected, considered optimal for enhanced scar visualization.

Table 1
Acquisition parameters for the 2D TI-scout and 2D SPOT sequences.

Sequence	TI-SCOUT	SPOT
Readout	2D bSSFP	
Preparation pulse	Inversion recovery and T1-rho	
Magnetic field (Tesla)	1.5	
Repetition time (ms)	2.9	
Echo time (ms)	1.2	
Flip angle (degrees)	60	
Field of view (mm)	380 × 315	
Acquired resolution (mm)	2.0 × 1.5 × 6.0	
Reconstructed resolution (mm)	1.5 × 1.5 × 6.0	
Phase oversampling (%)	0	
Slice oversampling	No	
Asymmetric echo	Yes	
Acquisition window (ms)	160	
T_1-rho duration (ms)	27	
T_1-rho frequency (Hz)	500	
Scan acceleration	GRAPPA x2	
Trigger pulse (RR interval)	2	
Bandwidth (Hz/pixel)	849	
Free-breathing	Yes	
Coverage	Mid-ventricular	Whole-heart
Number of slices (median [Q1-Q3])	1	14 [14–16]
Motion compensation	No	Yes
Inversion time range (ms)	60 – 190	n/a
Inversion time increment (ms)	10	n/a
Images per scout	14	n/a

Abbreviations: bSSFP, balanced steady-state free-precession; GRAPPA, generalized autocalibrating partially parallel acquisitions; GRE, gradient echo; n/a, not applicable; RR, time between two R waves.

2.3. Inline integration

The proposed algorithm was implemented inline on a 1.5 T MRI scanner using the Gadgetron framework [15]. The predicted TI value and a plot showing how the signal evolves with different TI values are sent back to the MR console for direct feedback to the MR operator. Supplementary Video 2 highlights the inline use of the proposed tool. The codes used to train the segmentation model as well as the Gadgetron gadget are made available at this repository: https://github.com/***/Automated-TI-scout.

2.4. Experiments

The study was approved by the Biomedical Research Ethics Committee and all participants provided informed consent for participation.

2.4.1. Imaging data

The feasibility and preliminary clinical performance of the proposed framework were assessed retrospectively in 329 patients with known or suspected heart disease. The dataset was split into:

i) A first set of 177 SPOT datasets (16 whole-heart short-axis SPOT slices per patient, 2177 images) to train, validate and test the

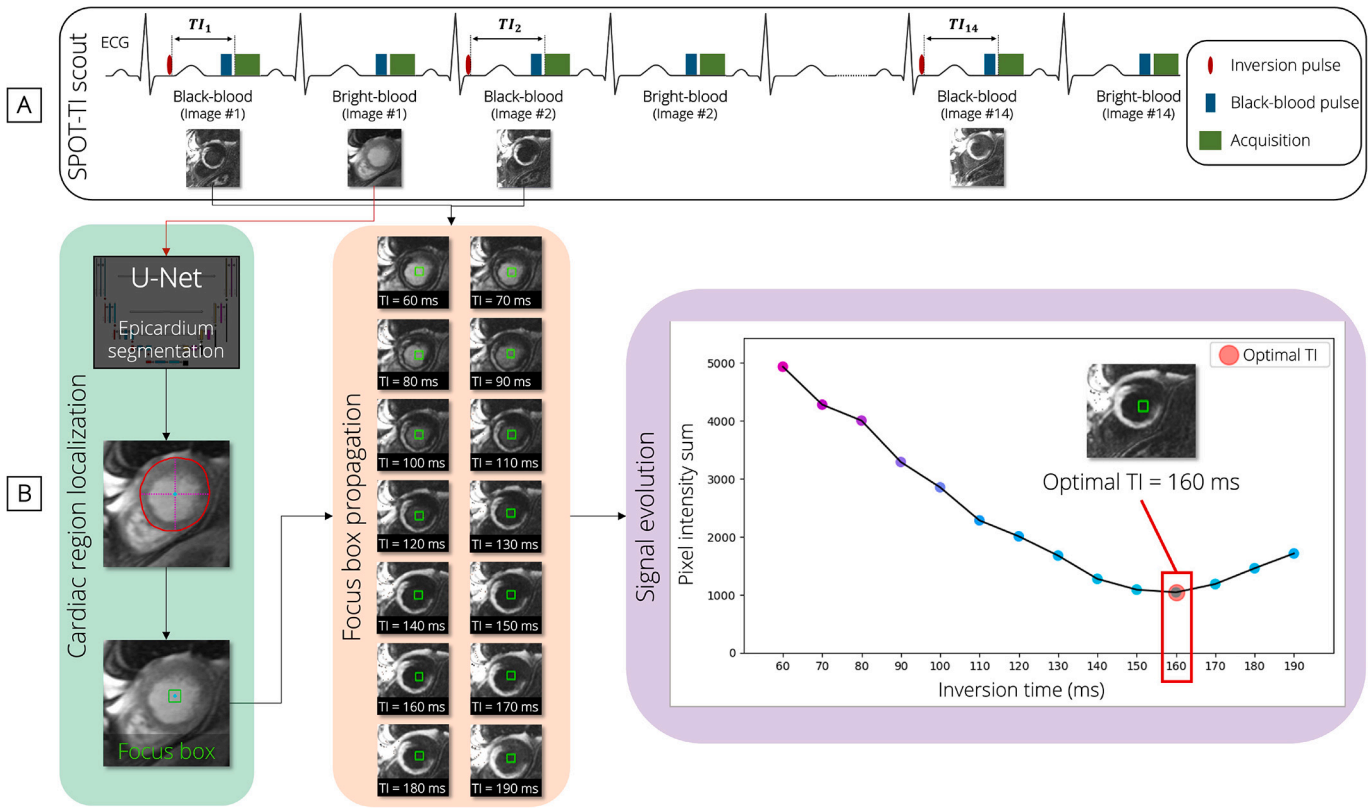

Fig. 1. Framework. A) TI-scout sequence B) Automatic epicardium segmentation on the first BR-LGE image obtained from the TI-scout. This segmentation was then used to create a focus box within the blood pool and was propagated on each BL-LGE image obtained from the TI-scout. The optimal TI corresponds to the minimum sum of pixel intensities. Abbreviations: TI, inversion time; BR, bright-blood; BL, black-blood; LGE, late gadolinium enhancement.

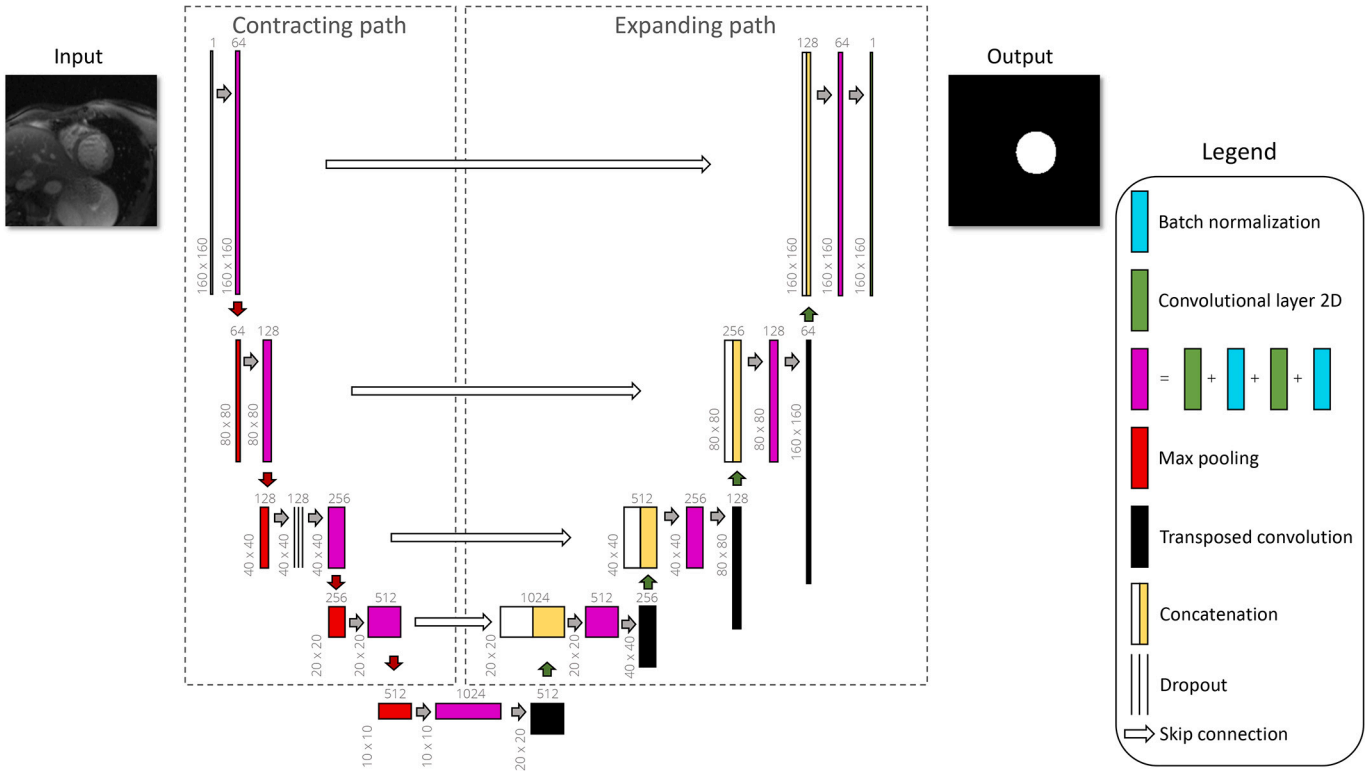

Fig. 2. Framework of the 2D U-Net architecture used to segment the epicardium. It is composed by two remain parts, a contracting path and an expanding path. The contracting path captures context information and reduces the spatial dimension of the input. The expanding path restores the spatial resolution and generates a segmentation map of the same size as the input image. The skip connections help to recover spatial details that may be lost during down sampling process.

proposed U-Net architecture for epicardium segmentation on BR-LGE images (25% female, 75% male, age 62 ± 13 years).

ii) A second set of 152 TI-scout datasets (14 mid-ventricular short-axis per patient, 2128 images), unseen during training, to validate the automated TI-scout selection framework (23% female, 77% male, age 59 ± 13 years).

2.4.2. U-Net training and LV segmentation validation

As mentioned earlier, the training and testing were performed on the first dataset (177 patients). Whole-heart epicardium labels were manually drawn for each patient by a cardiovascular magnetic resonance (MR) expert using the imaging software cvi42 (Circle Cardiovascular Imaging Calgary, Canada). The model's both input and output consisted of matrices with dimensions 160 × 160 × 1 (where the last number reflects the input channels). The number of images was increased with data augmentation (turning upside-down, left-right flips and 90°, 180°, 270° rotations) for a total of 13,760 images. The data was randomly divided into a training (70%, 123 patients, 9536 images), a validation (20%, 35 patients, 2776 images), and a test (10%, 19 patients, 1448 images) set, making sure images from a same patient were in the same set. Training was performed on a Dell PowerEdge R740 Server (Intel Xeon Gold 6154 3GHz, 18 cores, Python 3.9, Tensorflow 2.6), with the following hyperparameters: learning rate = 10^{-3}, batch size = 32, epochs = 200, binary cross-entropy loss, Adam optimizer. The Dice similarity coefficient [16] was used to evaluate the segmentation quality in the test set. The average Euclidean distance between manually-derived and model-derived LV centroids were reported.

2.4.3. Validation of predicted TIs

The second dataset (152 patients) was used to validate the automated TI selection framework. TI-scout images were visualized by two MR operators using cvi42 and reference TI values were recorded for each patient. A subsequent consensus value was provided in case of discrepancy. In addition to this, a consensus ±10 ms was also given, as for most cases the TI images surrounding the one selected (at $TI_{consensus}$ − 10 ms and $TI_{consensus}$ + 10 ms) provided a contrast difference visually undiscernible (as showcased in Supporting Information Fig. S1).

To test intra-observer reproducibility, the first MR operator provided an additional set of TI values in a separate session. On the other hand, the degree of confidence in the proposed algorithm was evaluated by conducting an extra TI selection by the second MR operator with now prior knowledge on the algorithm's TI prediction.

Intra- and inter-observer variability, consensus-algorithm and consensus±10 ms-algorithm agreements in TI selection were assessed using the Fleiss' kappa coefficient $\bar{\kappa}$. Kappa values below 0.4, between 0.4 and 0.75, and above 0.75 were considered to represent poor, fair to moderate, and excellent agreement, respectively, according to the Fleiss' classification. Mean absolute TI differences and percentages of matched TI values were calculated.

To assess the impact of the focus box size on the predicted TI, thirty different sizes ranging from 2.3mm^2 (1 × 1 pixel) to 20.3cm^2 (30 × 30 pixels) were tested on the whole dataset. The size that yielded the highest agreement value with the experts' consensus ±10 ms reading was selected for use in the subsequent experiments. Processing times were measured for one MR operator.

3. Results

3.1. LV segmentation quality

The U-Net model provided a Dice score of 93.0 ± 0.1% for the segmentation of the epicardium in the test dataset (19 patients). The average Euclidean distance between the manually-derived and model-derived LV centroids was 1.9 ± 1.6 mm (ranging from 0.0 mm to 14.6 mm, Fig. 3A and Supporting Information Fig. S3). Examples of automated epicardium segmentation on BR-LGE images with the corresponding LV centroids and focus boxes are shown in Fig. 4 for eight patients with ischemic heart disease.

3.2. Predicted TI results

The proposed algorithm extracted the TI value in an average of 2.7 ± 0.1 s per TI-scout, which was distinctly shorter than the average 16.0 ± 8.5 s needed for the visual extraction by the experts. Examples of automated LV segmentation, signal evolution within the focus boxes, and TI prediction are presented on Fig. 5 for three patients with ischemic heart disease.

Fleiss' kappa coefficient for experts, the consensus, and the algorithm in TI prediction agreements are presented in Table 2. There were fair to moderate intra- and overall inter-observers agreements in TI visual selection by the experts in the 152 patients ($\bar{\kappa} = 0.64$ and $\bar{\kappa} = 0.62$, respectively). A fair agreement ($\bar{\kappa} = 0.45$) was also obtained between the experts' consensus and the algorithm's predicted TI. However, an excellent agreement ($\bar{\kappa} = 0.89$) was obtained between the algorithm's prediction and the consensus ±10 ms (TI agreement in 137/152 TI-scouts). This coefficient was reached with an optimized focus box size of 2.3cm^2 (10 × 10 pixels) (Fig. 3B). The agreement was always excellent ($\bar{\kappa} > 0.75$) for focus box sizes ranging from 0.20cm^2 (3 × 3 pixels) to 20.25cm^2 (30 × 30 pixels).

The mean absolute differences in TI selection for inter-, intra-observer, consensus-algorithm and consensus±10 ms-algorithm variability were 5.0 ± 7.1 ms, 3.9 ± 6.2 ms, 6.2 ± 7.3 ms and 1.2 ± 4.0 ms, respectively (Fig. 6A, Supporting Information Fig. S4). The percentages of matched TI values for inter-observer, intra-observer, consensus-algorithm and consensus±10 ms-algorithm variability were 61.2%, 67.8%, 50.0% and 90.1%, respectively (Fig. 6B).

The second reading by the expert now having prior knowledge on the predicted TI modified its selection in 50% of the TI-scouts, reaching an excellent agreement ($\bar{\kappa} = 0.89$) with the algorithm's prediction.

4. Discussion

Accurate detection and quantification of myocardial injury using joint BR- and BL-LGE imaging has critical diagnostic and prognostic value in a wide range of patients presenting with heart diseases. Until now, no strategy has been proposed to fully automate contrast selection and enable TI extraction for this imaging technique, resulting in an operator-dependent task. Our proposed method enables an operator-free selection of TI for joint BR- and BL-LGE imaging.

4.1. TI prediction

Our results showed that the inter- and intra-expert agreement for manual TI selection was only fair to moderate. These results support the idea that manual selection of the optimal TI induces inter- and intra-expert variability and that a more reproducible selection is necessary. An incorrect selection of the TI can lead to suboptimal scar contrast, potentially influencing clinical decision. In such instances, it becomes necessary to repeat the LGE sequences with the accurate TI, significantly extending the protocol duration. The automated selection of the optimal TI demonstrated its potential by providing an excellent agreement with the consensus ±10 ms, in a faster fashion than manual TI selection.

4.2. Segmentation accuracy

The decision to perform an epicardium segmentation, rather than an endocardium segmentation, was based on empirical findings. Specifically, the epicardium mask prediction yielded a slightly better Dice score (detailed analysis not provided here). Additionally, during the extra validation phase, where we evaluated the accuracy of the centroids, four outliers with significantly higher Euclidian distances than the rest were observed. Despite the presence of these outliers, it is

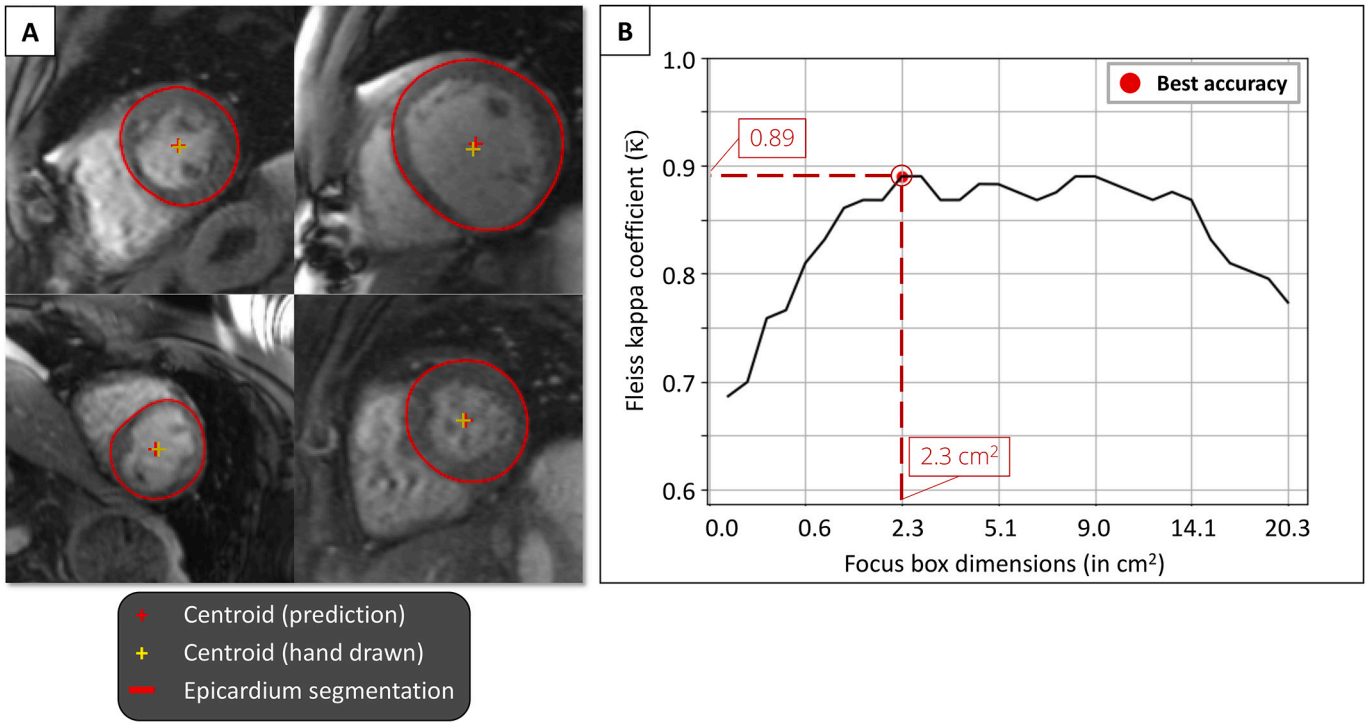

Fig. 3. A) Comparison between the centroids obtained from the ground truth segmentation (yellow cross) and from the proposed automated segmentation of the epicardium (red cross) for four representative SPOT BR-LGE images. B) Fleiss' kappa coefficient to assess the agreement between the consensus ±10 ms and the algorithm's TI prediction, as a function of the focus box dimensions. Abbreviations: SPOT, Scar-specific imaging with Preserved myOcardial visualizaTion; BR, bright-blood; LGE, late gadolinium enhancement. (For interpretation of the references to colour in this figure legend, the reader is referred to the web version of this article.)

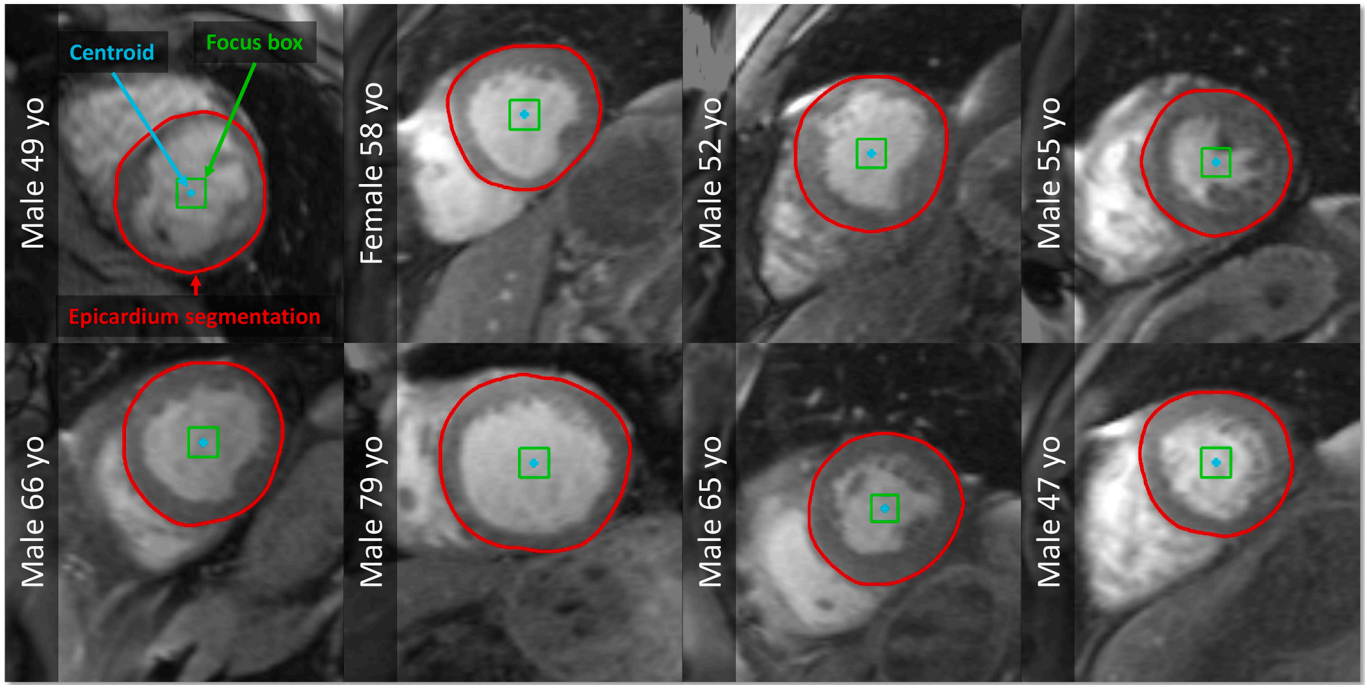

Fig. 4. Epicardial segmentation results (red) on SPOT BR-LGE images collected on eight different patients. The resulting focus boxes (green) and centroids (cyan) are also shown. Abbreviations: SPOT, Scar-specific imaging with Preserved myOcardial visualizaTion; BR, bright-blood; LGE, late gadolinium enhancement. (For interpretation of the references to colour in this figure legend, the reader is referred to the web version of this article.)

important to highlight that the focus box consistently remained within the blood pool, ensuring a correct extraction of the optimal TI.

4.3. Algorithm failures

The fifteen patients with incorrect TI prediction presented a successful epicardium segmentation. For ten out of these patients, it was

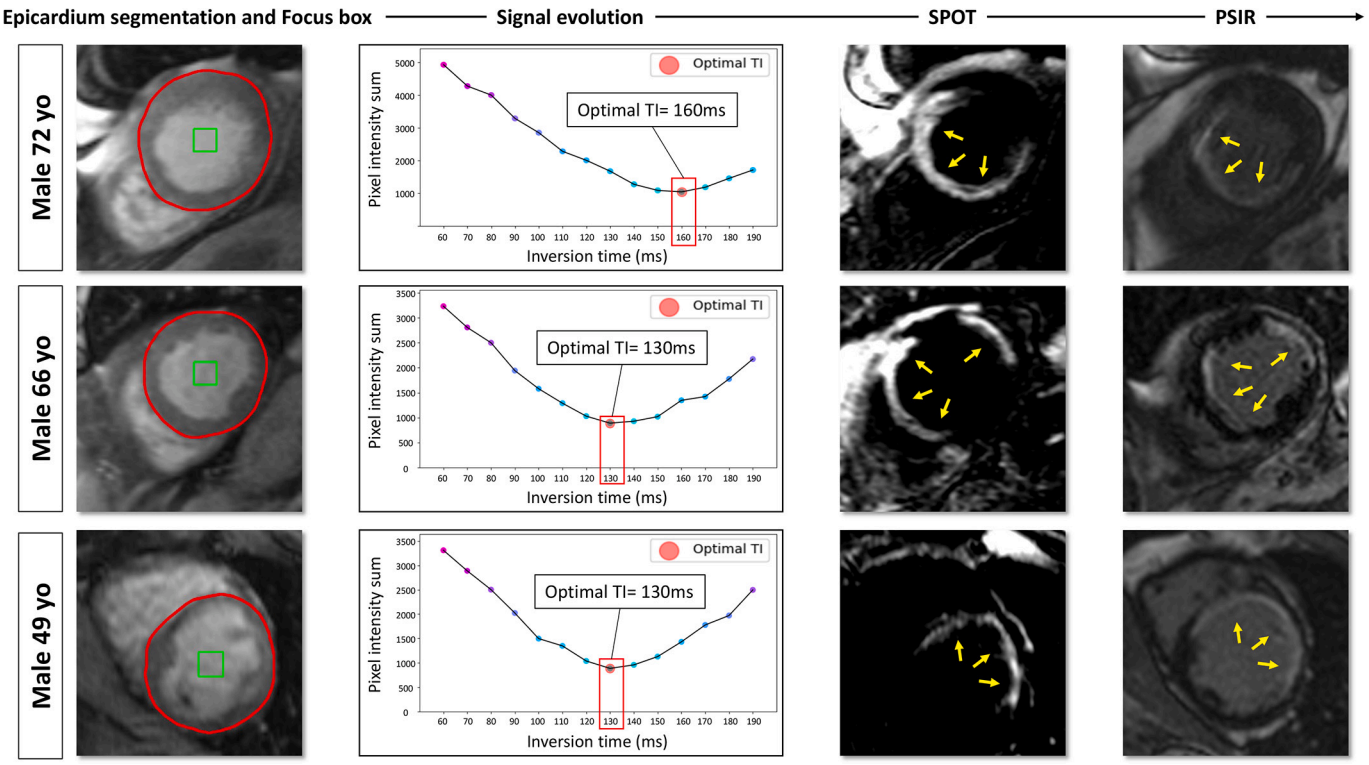

Fig. 5. Examples of inversion time (TI) predictions by the proposed fully automated algorithm, in three patients with ischemic heart disease. It is obtained by first creating a focus box centred on the predicted epicardium segmentation. This region of interest is then propagated on all BL-LGE images. The TI corresponding to the smallest pixel intensity sum inside the focus box is considered optimal. Abbreviations: PSIR, Phase-sensitive inversion recovery; SPOT, Scar-specific imaging with preserved myocardial visualization.

Table 2
Agreement table (computed using the Fleiss' kappa coefficient) between the MR operators (Expert 1, Expert 2) and the TI prediction, and between the experts' consensus and the TI prediction on a set of 152 TI-scout datasets. The agreements ranged from fair to moderate, to excellent. The highest agreement with the algorithm, obtained by the experts' consensus ±10 ms ($\bar{\kappa} = 0.89$), is highlighted. Manual expert selections are annotated as Expert X.Y for Expert X session Y. $^{\perp}$Intra-expert; $^{\circ}$Inter-expert.

	Expert 1.1	Expert 1.2	Expert 2.1	Expert 2.2 (with knowledge of prediction)	Experts' consensus	Experts' consensus ± 10 ms	Algorithm
Expert 1.1	1.00	0.64$^{\perp}$	0.57°	0.53	0.72	0.91	0.55
Expert 1.2		1.00	0.67°	0.50	0.65	0.94	0.48
Expert 2.1			1.00	0.47	0.85	0.99	0.46
Expert 2.2 (with knowledge of prediction)				1.00	0.45	1.00	0.89
Experts' consensus					1.00	1.00	0.45
Experts' consensus ± 10 ms						1.00	**0.89**
Algorithm							1.00

Note: $\bar{\kappa}$ Strength: $0.0 \leq \bar{\kappa} \leq 0.4$ Poor; $0.4 < \bar{\kappa} \leq 0.75$ Fair to moderate; $0.75 < \bar{\kappa} \leq 1.0$ Excellent.

observed that the predicted TI had a 20 ms difference (i.e., two TI images difference) with the experts' consensus. The algorithm's TI selection was based on a precise calculation of the pixel intensities, while the experts' consensus was based on a visual selection, resulting in a less accurate analysis. In the five remaining patients, it was discovered that the focus box contained pixels from necrosed papillary muscles. Consequently, this unintended inclusion led to a biased prediction in the TI estimation. To address this issue effectively, a potential solution would involve conducting a more comprehensive histogram-based analysis, following the methodology proposed by Maillot et al. [17].

4.4. Focus box optimization

As the TI-scout sequence was performed in free-breathing [5], respiratory motion could be observed between the different TI images. The main challenge therefore became defining an optimal focus box size that consistently encompassed pixels exclusively from the left ventricle, ensuring accurate TI analysis.

For this study, a squared shape focus box was selected, but further studies could explore the most optimal shape, such as a circular configuration, to enhance accuracy. Image registration could also be used to improve the accuracy. Hence, the focus box could have a bigger shape, as the images would be aligned, and take into account more pixels for the sum calculation.

4.5. Defining the algorithm's accuracy

Achieving optimal scar-to-blood and scar-to-healthy myocardium contrast requires the determination of an optimal TI. Consequently, the proposed algorithm was developed to select a single TI. Nonetheless,

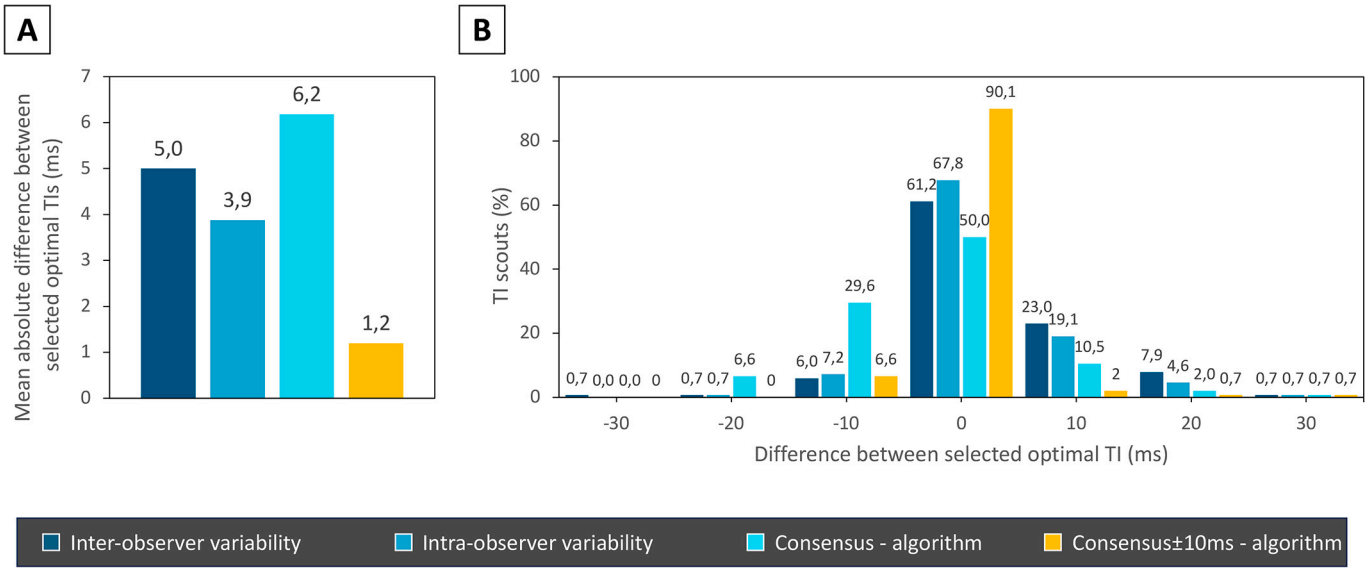

Fig. 6. Validation of the proposed automated TI selection algorithm by comparing consensus±10 ms-algorithm, consensus-algorithm, inter- and intra-observer variability on a set cohort of 152 TI-scouts. A) Mean absolute difference in inversion time (TI) selection. B) Percentage of matched scouts.

during the evaluation, it was noted that in certain TI-scouts, three to four TI images displayed a sufficiently black-blood signal, leading to acceptable contrast at the scar interface. The percentage difference of matched TI values between consensus-algorithm and consensus±10 ms-algorithm illustrates this statement. This observation highlights the challenge in quantifying the algorithm's accuracy, as defining what constitutes an acceptable contrast proves complex. Empirical findings showed that a difference of 10 ms with the expert's TI selection would not impact the corresponding TI image quality, hence the quantification of the injured myocardium and therefore the clinical decision.

Our results show that besides being fully automated, the proposed method brings several advantages compared to more conventional TI selection. Processing time was measured as being up to ten times faster than the time needed for manual selection. The workload was also reduced, and the variability in TI selection has been removed.

The optimal TI selection was tackled by comparing the intensity of the pixels located within a region of interest for each TI image and selecting the image and corresponding TI for which the sum was the lowest. Other techniques could have been chosen for this matter, for example by calculating the number of pixels whose values would be lower than a defined threshold [17].

The design of the proposed fully automated algorithm allows easy extension to other joint BR- and BL-LGE techniques. Indeed, the T1-rho pulse [12,18] has been chosen among many other preparation pulses that could have also been employed to generate black-blood images (e.g., T2 prep [19] and MTC [20]).

5. Conclusion

An algorithm allowing fully automated contrast selection for joint BR- and BL-LGE imaging was proposed. Accurate predictions of optimal TI values were obtained in a fast and fully automated fashion. The uncertainties, operator-dependency, and workload inherent to more conventional TI selection were reduced, while the inter- and intra-observer variability effects were removed. These promising results warrant larger and multi-center clinical validations.

Supplementary data to this article can be found online at https://doi.org/10.1016/j.mri.2024.03.035.

CRediT authorship contribution statement

Victor de Villedon de Naide: Writing – original draft, Writing – review & editing, Conceptualization, Methodology. **Jean-David Maes:** Writing – original draft, Writing – review & editing. **Manuel Villegas-Martinez:** Writing – original draft, Writing – review & editing. **Indra Ribal:** Writing – original draft, Writing – review & editing. **Valéry Ozenne:** Writing – original draft, Writing – review & editing, Software. **Géraldine Montier:** Writing – original draft, Writing – review & editing. **Thibaut Boullé:** Writing – original draft, Writing – review & editing. **Soumaya Sridi:** Writing – original draft, Writing – review & editing. **Pauline Gut:** Writing – original draft, Writing – review & editing. **Thomas Küstner:** Writing – original draft, Writing – review & editing. **Matthias Stuber:** Writing – original draft, Writing – review & editing. **Hubert Cochet:** Writing – original draft, Writing – review & editing, Data curation. **Aurélien Bustin:** Conceptualization, Funding acquisition, Writing – original draft, Writing – review & editing.

Acknowledgements

This research was supported by funding from the French National Research Agency under grant agreements Equipex MUSIC ANR-11-EQPX-0030, ANR-22-CPJ2-0009-01, ANR-21-CE17-0034-01, Programme d'Investissements d'Avenir ANR-10-IAHU04-LIRYC, and from the European Research Council (ERC) under the European Union's Horizon 2020 research and innovation program (grant agreement N°101076351).

References

[1] Kellman P, Arai AE, McVeigh ER, Aletras AH. Phase-sensitive inversion recovery for detecting myocardial infarction using gadolinium-delayed hyperenhancement. Magn Reson Med 2002;47(2):372–83. https://doi.org/10.1002/mrm.10051.
[2] Kim RJ, Fieno DS, Parrish TB, et al. Relationship of MRI delayed contrast enhancement to irreversible injury, infarct age, and contractile function. Circulation 1999;100(19):1992–2002. https://doi.org/10.1161/01.cir.100.19.1992.
[3] Hunold P, Schlosser T, Vogt FM, et al. Myocardial late enhancement in contrast-enhanced cardiac MRI: distinction between infarction scar and non-infarction-related disease. AJR Am J Roentgenol 2005;184(5):1420–6. https://doi.org/10.2214/ajr.184.5.01841420.
[4] Kim RJ, Wu E, Rafael A, et al. The use of contrast-enhanced magnetic resonance imaging to identify reversible myocardial dysfunction. N Engl J Med 2000;343(20):1445–53. https://doi.org/10.1056/NEJM200011163432003.

[5] Bustin A, Sridi S, Maillot A, et al. Improved myocardial scar visualization with two-minute free-breathing joint bright- and black-blood late gadolinium enhancement imaging. In: Proceedings from the joint annual meeting ISMRM-ESMRMB; 2022. p. 0271.
[6] Henningsson M, Malik S, Botnar R, Castellanos D, Hussain T, Leiner T. Black-blood contrast in cardiovascular MRI. J Magnet Reson Imaging 2022;55(1):61–80. https://doi.org/10.1002/jmri.27399.
[7] Holtackers RJ, Heyning CMVD, Chiribiri A, Wildberger JE, Botnar RM, Kooi ME. Dark-blood late gadolinium enhancement cardiovascular magnetic resonance for improved detection of subendocardial scar: a review of current techniques. J Cardiovasc Magn Reson 2021;23(1):96. https://doi.org/10.1186/s12968-021-00777-6.
[8] Ginami G, Neji R, Phinikaridou A, Whitaker J, Botnar RM, Prieto C. Simultaneous bright- and black-blood whole-heart MRI for noncontrast enhanced coronary lumen and thrombus visualization. Magn Reson Med 2018;79(3):1460–72. https://doi.org/10.1002/mrm.26815.
[9] Gassenmaier S, van der Geest RJ, Schoepf UJ, et al. Quantitative inversion time prescription for myocardial late gadolinium enhancement using T1-mapping-based synthetic inversion recovery imaging: reducing subjectivity in the estimation of inversion time. Int J Card Imaging 2018;34(6):921–9. https://doi.org/10.1007/s10554-017-1294-9.
[10] Bahrami N, Retson T, Blansit K, Wang K, Hsiao A. Automated selection of myocardial inversion time with a convolutional neural network: spatial temporal ensemble myocardium inversion network (STEMI-NET). Magn Reson Med 2019;81(5):3283–91. https://doi.org/10.1002/mrm.27680.
[11] Schmidt M, Rick M, Chitiboi T, et al. Validation of a deep learning based automated myocardial inversion time selection for late gadolinium enhancement imaging in a prospective study. In: Vol international society for magnetic resonance in medicine (ISMRM) 29th annual meeting & exhibition; 2021. Abtract n°452, https://index.mirasmart.com/ISMRM2021/PDFfiles/0452.html.
[12] Sridi S, Nuñez-Garcia M, Sermesant M, et al. Improved myocardial scar visualization with fast free-breathing motion-compensated black-blood T1-rho-prepared late gadolinium enhancement MRI. In: Diagnostic and interventional imaging; 2022. https://doi.org/10.1016/j.diii.2022.07.003. Published online August.
[13] Messroghli DR, Moon JC, Ferreira VM, et al. Clinical recommendations for cardiovascular magnetic resonance mapping of T1, T2, T2* and extracellular volume: a consensus statement by the Society for Cardiovascular Magnetic Resonance (SCMR) endorsed by the European Association for Cardiovascular Imaging (EACVI). J Cardiovasc Magn Reson 2017;19(1):75. https://doi.org/10.1186/s12968-017-0389-8.
[14] Ronneberger O, Fischer P, Brox T. U-net: convolutional networks for biomedical image segmentation. In: Medical image computing and computer-assisted intervention; 2015. p. 234–41. https://doi.org/10.1007/978-3-319-24574-4_28. Published online.
[15] Hansen MS, Sørensen TS. Gadgetron: an open source framework for medical image reconstruction. Magn Reson Med 2013;69(6):1768–76. https://doi.org/10.1002/mrm.24389.
[16] Measures of the amount of ecologic association between species. Ecology 1945;26(3):297–302. https://doi.org/10.2307/1932409.
[17] Maillot A, Sridi S, Pineau X, et al. Automated inversion time selection for black-blood late gadolinium enhancement cardiac imaging in clinical practice. MAGMA 2023. https://doi.org/10.1007/s10334-023-01101-2. Published online June.
[18] Muscogiuri G, Rehwald WG, Schoepf UJ, et al. T(rho) and magnetization transfer and INvErsion recovery (TRAMINER)-prepared imaging: a novel contrast-enhanced flow-independent dark-blood technique for the evaluation of myocardial late gadolinium enhancement in patients with myocardial infarction. J Magn Reson Imaging 2017;45(5):1429–37. https://doi.org/10.1002/jmri.25498.
[19] Kellman P, Xue H, Olivieri LJ, et al. Dark blood late enhancement imaging. J Cardiovasc Magn Reson 2016;18(1):77. https://doi.org/10.1186/s12968-016-0297-3.
[20] Kawata H, Nishimura H, Nagata S, Matsuda T, Takada K, Hayabuchi N. Fundamental study of magnetization transfer contrast (MTC) effect: optimization of MT pulse condition using experimental phantom. Nihon Hoshasen Gijutsu Gakkai Zasshi 2004;60(10):1437–43. https://doi.org/10.6009/jjrt.kj00003326546.